

The Devil Is in the Details: What Do We Really Track in Single-Particle Tracking Experiments of Diffusion in Biological Membranes?

Andrey A. Gurtovenko,^{*,†,‡,§} Matti Javanainen,^{¶,§,||} Fabio Lolicato,^{¶,§} and Ilpo Vattulainen^{¶,§,⊥}

[†]Institute of Macromolecular Compounds, Russian Academy of Sciences, Bolshoi Prospect V.O. 31, St. Petersburg 199004, Russia

[‡]Faculty of Physics, St. Petersburg State University, Ulyanovskaya Street 3, Petrodvorets, St. Petersburg 198504, Russia

[¶]Department of Physics, University of Helsinki, P.O. Box 64, FI-00014 Helsinki, Finland

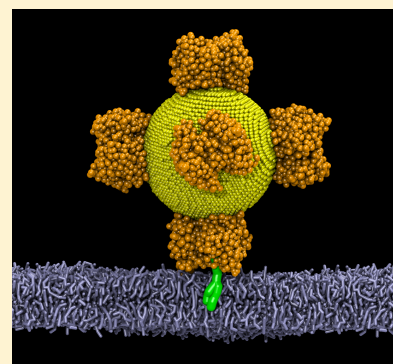
[§]Computational Physics Laboratory, Tampere University, P.O. Box 692, FI-33014 Tampere, Finland

^{||}Institute of Organic Chemistry and Biochemistry of the Czech Academy of Sciences, Flemingovo náměstí 542/2, 166 10 Prague 6, Czech Republic

[⊥]MEMPHYS—Center for Biomembrane Physics, Denmark

Supporting Information

ABSTRACT: Single-particle tracking (SPT) is an experimental technique that allows one to follow the dynamics of individual molecules in biological membranes with unprecedented precision. Given the importance of lipid and membrane protein diffusion in the formation of nanoscale functional complexes, it is critical to understand what exactly is measured in SPT experiments. To clarify this issue, we employed nanoscale computer simulations designed to match SPT experiments that exploit streptavidin-functionalized Au nanoparticles (AuNPs). The results show that lipid labeling interferes critically with the diffusion process; thus, the diffusion measured in SPT is a far more complex process than what has been assumed. It turns out that the influence of AuNP-based labels on the dynamics of probe lipids includes not only the AuNP-induced viscous drag that is the more significant the larger the NP but, more importantly, also the effects related to the interactions of the streptavidin linker with membrane lipids. Due to these effects, the probe lipid moves in a concerted manner as a complex with the linker protein and numerous unlabeled lipids, which can slow down the motion of the probe by almost an order of magnitude. Furthermore, our simulations show that nonlinker streptavidin tetramers on the AuNP surface are able to interact with the membrane lipids, which could potentially lead to multivalent labeling of the NPs by the probe lipids. Our results further demonstrate that in the submicrosecond time domain the motion of the probe lipid is uncorrelated with the motion of the AuNP, showing that there is a 1 μ s limit for the temporal resolution of the SPT technique. However, this limit for the temporal resolution depends on the nanoparticle size and increases rapidly with growing AuNPs. Overall, the results provide a molecular-scale framework to accurately interpret SPT data and to design protocols that minimize label-induced artifacts.



Cell membranes, being essentially lipid bilayers hosting membrane proteins, represent quite unique two-dimensional interfaces, where numerous cellular functions take place.¹ Cellular processes are typically regulated by membrane proteins that in turn are modulated by lipids. Understanding the formation of functional protein–lipid complexes is a central step in understanding how cellular functions originate and take place.^{2,3} If the formation of protein–lipid complexes is compromised, then the related cellular functions are impaired, and this can have severe consequences that are often related to the onset of diseases. The most relevant dynamic process in this context is the lateral diffusion of proteins and lipids in the membrane plane because it governs the formation of protein–lipid complexes and is involved in, e.g., protein sorting, signaling transduction, and cell death.^{4,5} Given this, it is of outstanding importance to understand how lipids and proteins diffuse in membranes in the nanoscale, thereby forming functional complexes.

A key to the studies of lateral diffusion in model and cell membranes is the development of noninvasive experimental techniques that render the imaging of the motion of individual lipids and proteins possible. Recent advances in this area are closely related to single-particle tracking (SPT).^{6–9} In a typical SPT experiment, a biomolecule of interest is first labeled with a nanoscopic optical label, whose motion is then imaged by a light microscopy technique. Both fluorescent (fluorescent dyes and quantum dots) and nonfluorescent (gold nanoparticles, AuNPs) probes could be used as labels in SPT; in the latter case, the imaging is based on light scattering.^{8,10} Although some of the labels can be attached directly to a biomolecule, in most cases, one needs a specific linker, a so-called “specificity module” according to the terminology proposed in ref 10.

Received: January 9, 2019

Accepted: February 15, 2019

Published: February 15, 2019

These modules include, e.g., full antibodies, Fab fragments, streptavidin (sAv), and cholera toxin subunit B.^{8,10}

One of the major drawbacks of the SPT approach is related to possible label-induced artifacts. In particular, the perturbations arising from the optical labels can be very problematic given that one of the primary objectives of using SPT is to unravel the genuine dynamics of lipids and proteins on the nanoscale. If the labels altered the dynamics of the labeled molecules or the membrane, then the data given by SPT experiments would be tough to interpret. This problem is more than likely because AuNPs and quantum dots are 5–50 times larger than the lipids to which they are attached.¹⁰

Fortunately, recent developments of the SPT techniques have reached the stage where one can image the motion of individual molecules with exceptional resolution, so that experimental data can now be directly linked with state-of-the-art computer simulations. An excellent example of these techniques is high-speed interferometric scattering (iSCAT) microscopy.^{11–14} To track how lipid molecules move in membranes, high-speed iSCAT investigations often employ AuNPs as optical labels. A typical diameter of AuNPs lies in the range of 20–40 nm,^{11,12,15} although the use of AuNPs as small as 5 nm has also been reported.¹³ With the use of such labels, iSCAT microscopy allows one to follow the motion of single lipids with simultaneous nanometer spatial and microsecond temporal resolution.^{13,14} Such time and length scales are currently accessible by computer simulations.

In this Letter, we use nanoscale computer simulations to unravel the complex membrane dynamics measured in SPT experiments. The primary aim is to clarify what exactly is measured when SPT is applied to study lipid dynamics. The results show that the diffusion of lipid probes measured by SPT is a far more complex process than what has been assumed. For the purposes of our study, we focused on labeling lipid molecules with sAv-functionalized AuNPs.

We performed molecular dynamics (MD) simulations using models that match conditions explored in iSCAT measurements. We considered a single biotinylated probe lipid (dipalmitoyl-phosphoethanolamine-*N*-(cap biotinyl) (biotin-cap-DPPE)) embedded in a palmitoyl-oleoyl-phosphatidylcholine (POPC) bilayer. The biotinylated DPPE probe was attached to a AuNP via a sAv tetramer linker,¹⁰ which is used in experiments to establish tight binding between AuNPs and biotinylated probe phospholipids embedded in a lipid membrane.^{13–15} We considered AuNPs of two sizes. The smaller one (5 nm in diameter) hosted a single sAv tetramer, while the larger AuNP (10 nm) hosted six tetramers, matching experimental conditions;¹¹ see Figure 1A,B. In experiments, AuNPs are typically about 20–40 nm in size, but for the sake of feasibility, in our simulations, we focused on smaller nanoparticles. To access the microsecond time scale and spatial scales of 10s of nanometers, we employed the coarse-grained Martini force field.^{16–18} All systems were simulated in an *NpT* ensemble at $T = 310$ K and $p = 1$ bar. To improve statistical reliability of results, every system (except the controls) was studied through three replica simulations, each being 50 μ s long (Table 1). The total time scale of the simulations was about 500 μ s. The GROMACS 5.1.4 suite was used to perform the simulations.¹⁹ For details regarding the model systems, the setup, and the simulations, see the Supporting Information (SI).

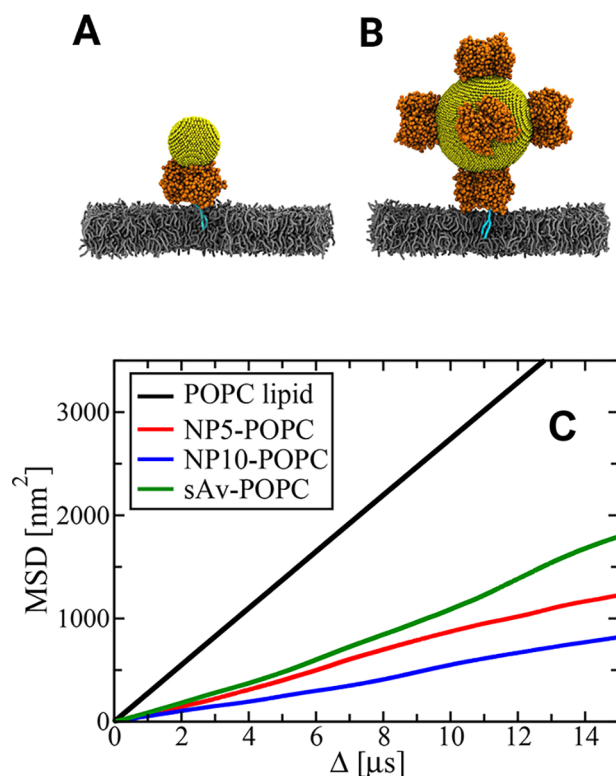


Figure 1. Snapshots of POPC lipid bilayers hosting a probe lipid labeled with sAv-functionalized AuNPs, whose diameters are (A) 5 or (B) 10 nm. POPC bilayers are shown in gray, probe biotin-cap-DPPE lipids in cyan, sAv tetramers in orange, and AuNPs in yellow. (C) Mean-squared displacements (MSDs) of label-free and labeled lipids as a function of lag time Δ . For the labeled lipids, data are shown for AuNPs, whose sizes are 5 or 10 nm as well as for sAv. The MSD for the label-free lipids was averaged over 2048 POPC lipids; the MSD for the labeled lipids was averaged over three independent simulations (50 μ s each).

Table 1. Description of the Simulated Systems^a

system	NP diameter [nm]	simulated time scale [μ s]
NP10-POPC	10	3×50
NP5-POPC	5	3×50
sAv-POPC		3×50
DPPE-POPC		50
POPC-2048		50

^aThe system POPC-2048 contained only a membrane composed of POPCs, and the system DPPE-POPC contained DPPE lipids (0.5 mol % of DPPE) embedded in a POPC membrane. These two systems acted as controls. The system sAv-POPC contained the POPC membrane and a single biotinylated DPPE lipid attached to a sAv tetramer. The systems NP5-POPC and NP10-POPC were based on sAv-POPC but contained also one AuNP attached to the sAv tetramer.

As in experiments, the lateral diffusion coefficient D is extracted here from the mean-squared displacement (MSD) at long times according to the Einstein relation

$$D = \lim_{\Delta \rightarrow \infty} \text{MSD}(\Delta)/4\Delta$$

where Δ is the lag time and $\text{MSD}(\Delta) = \frac{1}{N} \sum_1^N \text{MSD}_i(\Delta)$, averaged over N particles, simulation time t_{sim} , and replica simulations when possible. The time averaging is performed for each particle i as $\text{MSD}_i(\Delta) =$

$\frac{1}{t_{\text{sim}} - \Delta} \int_0^{t_{\text{sim}} - \Delta} dt [\vec{r}(t + \Delta) - \vec{r}(t)]^2$, where $\vec{r}(t)$ is the position of the particle at time t .

Figure 1C and Table 2 summarize the first primary finding of this work: labeling significantly slows down the lateral

Table 2. Diffusion Coefficients D of the Label-Free and Labeled Lipids^a

system	D [10^{-7} cm ² /s]	N_{lipids}	L_{domain} [nm]
NP10–POPC	1.28 ± 0.08	12.1 ± 2.3	6.34 ± 0.90
NP5–POPC	1.85 ± 0.23	12.5 ± 2.3	6.48 ± 0.80
sAv–POPC	2.32 ± 0.34	12.1 ± 2.3	6.46 ± 0.78
DPPE–POPC	7.06 ± 0.13		
POPC-2048	6.86 ± 0.02		

^aIn POPC-2048, D describes the diffusion of POPC lipids. In DPPE–POPC, D is measured for unlabeled DPPE lipids embedded in a POPC membrane. In sAv–POPC, D is for the biotinylated DPPE linked to the sAv tetramer. In NP5–POPC and NP10–POPC, the diffusion data are given for the biotinylated DPPE linked to the sAv tetramer, which in turn is attached to the AuNP. L_{domain} stands for the diameter of a lipid domain beneath the sAv linker, and N_{lipids} is the average number of lipids in that domain. The errors correspond to the standard error.

diffusion. The diffusion coefficient of a probe lipid labeled with a 5 nm AuNP is ~ 3.7 times smaller than the diffusion coefficient of label-free lipids (Table 2). When the size of the AuNP is increased, the disparity becomes even more pronounced: labeling a lipid with a functionalized 10 nm AuNP slowed down its lateral diffusion by a factor of ~ 5.4 . Meanwhile, the diffusion coefficient of label-free POPC was found to be $(6.86 \pm 0.02) 10^{-7}$ cm²/s, in good agreement with previous simulation studies^{20,21} that employed the Martini force field. We confirmed that label-free DPPEs embedded in a POPC membrane demonstrate the same diffusive behavior as POPCs (see Table 2); thus, only POPCs will be discussed in the following as unlabeled (control) lipids. Notably, most experimental papers have discussed mainly the differences between normal and confined modes of diffusion,⁷ although some studies have also reported the absolute values of diffusion coefficients.^{13,14} Here we focus on the Brownian diffusion only, whereas the subdiffusive behavior²² will be a subject of a separate study.

The AuNP interferes with the diffusion of the lipid to which it is attached, but the effect is only local. This view is backed up by the data showing that the diffusion coefficients of label-free POPC lipids are similar: embedding a labeled lipid into a membrane results in just a slight change in the diffusion of the POPCs (Table S2). This indicates that the viscosities of the membranes are not significantly altered by the introduction of the labeled lipid.

To figure out the key factors causing the major drop in the lateral diffusion of AuNP-labeled lipids, we carried out additional NP-free simulations using a system (sAv–POPC in Table 1) in which the biotinylated DPPE probe was linked to only the sAv tetramer (without AuNP). The results shown in Figure 1C and Table 2 highlight the quite surprising finding that the sAv linker alone slows down the lateral diffusion of the labeled lipid by a factor of ~ 3 . In other words, for nanoparticles of the considered size (5 and 10 nm in diameter), a significant share of the effect of labeling on lateral diffusion arises from the sAv linker and not from the drag on the nanoparticle itself. Moreover, as discussed below,

this drag is probably overestimated in simulations, indicating that in reality the effect of the sAv–membrane interaction dominates the slowing down of the diffusion of the labeled lipid. This phenomenon, to our knowledge, has not been previously reported.

Why does the sAv tetramer slow down the diffusion of its host lipid, and how does it do it? The answers to these questions are illustrated in Figure 2, which depicts how sAv

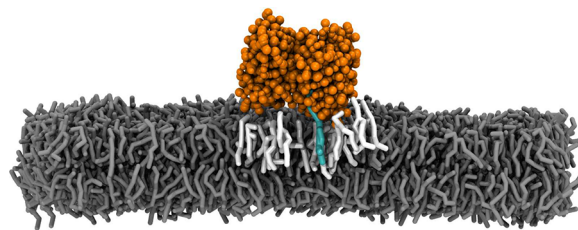


Figure 2. Snapshot of a probe lipid (cyan) labeled with the sAv tetramer (orange) within the POPC lipid bilayer (gray). POPC lipids that interact with the sAv tetramer are highlighted in white.

interacts with the lipids that are underneath of it. To characterize these interactions and their effects, we first determined the lipids that are in contact with sAv. A lipid molecule was considered to establish a contact with sAv if the lipid head group beads were within 0.6 nm from any of the protein's residues. It turned out that sAv interacts on average with ~ 12 POPCs (Table 2 and Figure 3A) that diffuse together with sAv. In other words, the probe lipid that is linked to sAv does not move alone but diffuses together with a lipid domain comprised of a dozen neighboring lipids (Figure 2), which explains the observed slowdown.

On the basis of lipids interacting with sAv, the average size of the lipid domain, L_{domain} , is about 6.5 nm (Figure 3A and Table 2). An alternative way to evaluate the size of this domain is to identify the lipids that move together with sAv.²¹ To this end, we calculated the mean in-plane displacements of lipids over a 1 ns interval as a function of distance from the probe lipid. Using an analogy to the diffusion of lipids in the vicinity of a transmembrane protein,²³ we expect the lipids next to the sAv-bound probe lipid to move slowly and the movement of lipids to speed up as their distance from the probe lipid increases. This is also what we observe (Figure 3B). On the basis of this approach, the size (diameter) of the dynamically coupled lipid domain ranges between 5 and 8 nm, which is in reasonable agreement with L_{domain} .

The diffusion coefficient of the sAv-bound lipid domain can be estimated with the Saffman–Delbrück (SD) model,²⁴ which was recently extended to objects spanning a single leaflet²⁵ and to systems with periodic boundary conditions (PBCs).^{25,26} The SD model predicts the diffusion coefficients to scale fairly weakly as $D \approx \ln L_{\text{domain}}^{-1}$. This model, when applied to the domain motion in the sAv–POPC system and taking into account the interleaflet friction, predicts that the diffusion coefficient of the lipid domain with a diameter of 6.5 nm is ~ 4.5 times smaller compared to that of a single lipid, in fair agreement with the observed decrease of ~ 3 . Extrapolating the diffusion coefficients to infinite systems,^{25,26} the ratio remains substantial at ~ 2.7 .

Turning now from the impact of sAv to the influence of the nanoparticle size, a comparison of the diffusion coefficients of sAv–POPC and NP–POPC systems clearly indicates that the

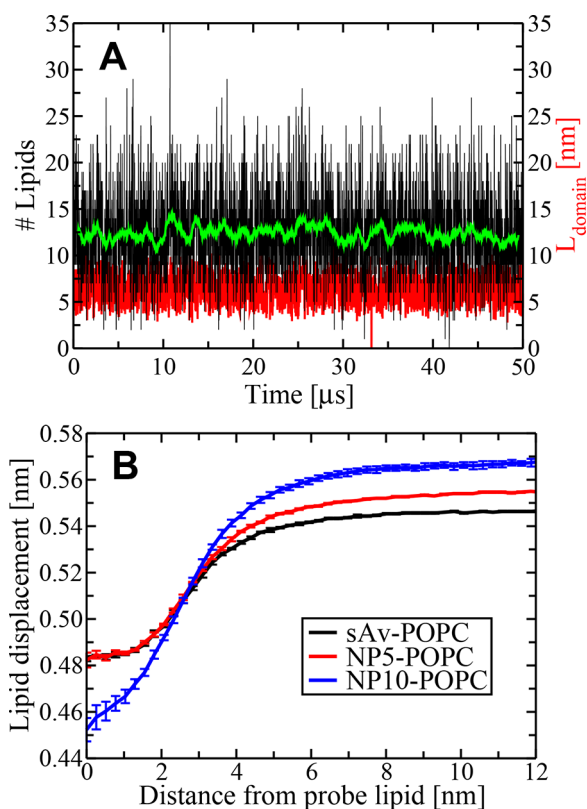


Figure 3. (A) Time evolution (along with its running average) of the number of lipids bound to the sAv linker (black and green curves) and of the size (diameter) L_{domain} of the corresponding lipid domain for the sAv-POPC system (red curve). (B) Average in-plane displacements of lipids as a function of distance from the probe lipid, which is $1/2$ of the domain size L_{domain} .

presence of AuNP leads to an additional decrease in the diffusion of the probe lipid (Table 2). This decrease correlates with the size of the NP: the larger the AuNP, the more it slows down the lateral diffusion of the probe lipid. This finding also implies that considering nanoparticles larger than those studied in this paper (5 and 10 nm in diameter) could lead to the situation where the effects of the sAv linker and the nanoparticle size become comparable.

What causes this dependence on the NP size? The number of lipids bound to sAv does not depend on AuNP size (Table 2). The height of the solvent layer is known to have a weak effect on diffusion coefficients;^{25–28} however, with our simulation box sizes, this effect is also irrelevant.^{25,26} This view is also supported by the almost identical diffusion coefficients of POPC in all of the simulated systems (Table S2).

Obviously, in our simulations, the influence of the NP size on the lateral diffusion is due to the frictional drag of a nanoparticle moving in a viscous medium such as water. Essentially, a NP experiences the friction force from the solvent molecules; this force affects its mobility and correspondingly the mobility of the probe lipid. The diffusion coefficient of a 3D object having a hydrodynamic radius R_{H} in a viscous medium scales as R_{H}^{-1} , implying that the significance of the frictional drag increases for increasing nanoparticle size. This size dependence of the frictional drag leads to a slowdown in the lateral diffusion from 3 to 3.7 times for a 5 nm AuNP and to 5.4 times for its 10 nm counterpart.

However, we note that in real membrane systems the viscosity of the membrane is ~ 100 times larger than the viscosity in the surrounding aqueous solution.¹⁰ In the Martini model, the viscosity of the membrane is only ~ 10 times larger than the viscosity of the water phase.^{16,21} This indicates that any viscous drag in the aqueous phase observed in simulations is overestimated and further highlights the sAv-membrane interaction as the major contributor to the observed slow diffusion of the labeled lipid.

One feature of the sAv-functionalized AuNPs considered here is that only one sAv tetramer on the 5 nm NP is linked to a (single) probe lipid. This is also the case for one of the sAv tetramers on the 10 nm NP, while the other sAv tetramers on the 10 nm NP are not linked to other biotinylated lipids. Therefore, neither multivalent labeling at a single sAv tetramer nor the lipid cross-linking by multiple sAvs on a NP are considered. However, both situations can be encountered in experiments if special care is taken to ensure the monovalent binding of the NP to a single probe lipid. This can be achieved, e.g., by saturating sAv binding sites by adding an excess amount of biotin molecules¹⁴ or by minimizing the amount of linker agents (such as Fab fragments) on the surface of AuNPs.²⁹

Indeed, our simulations of lipid bilayers with a 10 nm AuNP clearly show that in case the NP is large enough to host several sAv linkers on its surface lipid cross-linking can readily take place. It has been shown that as the NP size increases the number of sAv tetramers on its surface also increases.¹¹ For a NP that is about 10 nm in size, the number of sAv tetramers on its surface is expected to be around 5–6.¹¹ One of these tetramers is obviously linked to the probe lipid through biotinylation. However, given that in experiments the molar fraction of biotinylated probe lipids can be as large as 1 mol %, ¹⁴ it is tempting to ask whether several of the sAv tetramers on the nanoparticle surface could interact with biotinylated probe lipids or other membrane lipids at the same time?

While the aforementioned experimental procedures aim to prevent the cross-linking of the NP by biotinylated lipids, our results show that a more general interaction is also possible. As exemplified in Figures 1B and 4, we found that quite frequently the functionalized AuNP touches the surface of the lipid bilayer from several different locations. One of the contacts is

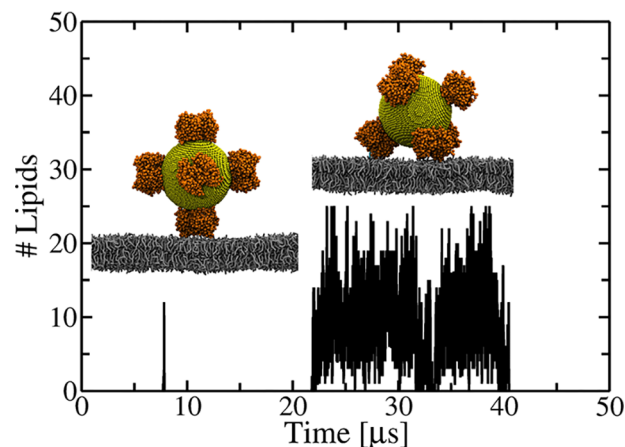


Figure 4. Time evolution of the number of lipids that are in contact with nonlinker sAv tetramers of a 10 nm AuNP.

directed to the biotinylated probe lipid. In the other cases, sAv tetramers are transiently exposed to contacts with POPCs (Figure 4). Therefore, if the NP size is large enough, thus rendering the binding of several sAv tetramers to its surface possible, then the nonlinker sAv tetramer can establish a contact with biotinylated probe lipids or a transient contact with other membrane lipids. As a matter of fact, multivalent binding of sAv-functionalized AuNPs is often considered one of the key artifacts in SPT experiments.³⁰ Given this, our findings provide compelling evidence for the conclusion that the diameter of the AuNP should be as small as possible to minimize NP-related artifacts.

Now assuming that the NP size is sufficiently small (about 5 nm) to exclude effects of multivalency, then how well does the trajectory given by SPT describe the trajectory of the probe molecule? This question is relevant given that the SPT trajectory can be used to deduce information about membrane structure¹⁴ as well as about the diffusion mechanism.^{31,32} However, such analyses are meaningful only if the measured trajectory of the NP also describes the motion of the probe lipid. We therefore explored the correlation between the motion of the NP and the labeled lipid by calculating their MSDs (Figures 5A and S1). The data reveal that both the NP and the labeled lipid reach the regime of normal diffusion at Δ

$\approx 0.5 \mu\text{s}$ and that their diffusion coefficients are essentially identical. This somewhat expected result confirms that the diffusion coefficients measured by SPT really describe the motion of the labeled lipid in the long-time Brownian regime.

However, the situation is very different at shorter time scales. To unravel how strongly the motions of the NP and the probe lipid are correlated, we studied this problem as follows. For each time interval $\Delta t \geq 0$, we calculated the correlation between the displacements of the labeled lipid, $\delta\vec{r}(t, \Delta t) = \vec{r}(t + \Delta t) - \vec{r}(t)$, and the NP, $\delta\vec{R}(t, \Delta t) = \vec{R}(t + \Delta t) - \vec{R}(t)$, where $\vec{r}(t)$ and $\vec{R}(t)$ are the 2D positions of the labeled lipid and the NP projected to the membrane surface (see the SI for details). Averaging was performed over the trajectory in order to obtain the correlation as a function of lag time Δ .

Figure 5B depicts the correlation between the movements of the labeled lipid and the NP, together with the standard error calculated over the replicas. A fully correlated movement of the labeled lipid and the NP corresponds to the correlation being about 1. Meanwhile, the closer this value is to zero, the weaker the correlation.

For the 5 nm AuNP, its short-time dynamics is almost uncorrelated with the dynamics of the labeled lipid (Figure 5B). The correlation grows with increasing lag time and reaches a value of 0.8 in about 200–300 ns and a plateau with a value of ~ 0.9 when the lag time is on the order of 1 μs . These results indicate that if the sampling rate of the NP position is less frequent than $1 \mu\text{s}^{-1}$ then the trajectory of the NP reflects the trajectory of the labeled probe lipid. However, if the sampling rate is more frequent than $1 \mu\text{s}^{-1}$, then the interpretation of the NP trajectory can be problematic.

For the larger 10 nm AuNP, the results are, to a great extent, similar to those of the 5 nm AuNP (Figure 5B). The main difference regards the time scale because in the 10 nm AuNP system the development of the correlation takes longer. Here, the correlation reaches a value of 0.8 in about 5–10 μs . Thus, for AuNPs of this size, the sampling of the nanoparticle position should be done at a rate of about $10 \mu\text{s}^{-1}$ or less frequently; otherwise, the NP trajectory would not describe the motion of the probe lipid to a satisfactory degree.

The results presented here set a natural limit for the temporal resolution of SPT techniques in general (and the iSCAT microscopy in particular): going to the submicrosecond time domain is not a particularly sensible goal because the movement of the NP cannot be linked to the dynamics of the labeled lipid in a reliable manner. For the 10 nm AuNP system, the results actually suggest sampling of the NP position to be done once every 10 μs . While in this work we did not study larger NPs, the results suggest that the sampling rate should then be even slower. We note that, while most SPT studies are far from the above-mentioned temporal limit, some state-of-the-art iSCAT experiments approach the temporal resolution of 10 μs .^{13,15}

In summary, here we presented and discussed the results of the first in silico study that provides a molecular-scale view into the process measured in SPT. In SPT experiments, one follows the motion of probe molecules that are linked to nanoparticles. One of the means to exploit this concept is to use lipids whose head group is linked to biotin, which in turn binds to sAv tetramers attached to the surface of a AuNP. By following the trajectory of the AuNP, one can trace the dynamics of the probe molecule with nanoscale spatial resolution. However, our results show that this labeling strategy has significant effects on the lateral diffusion of the labeled lipids. The first

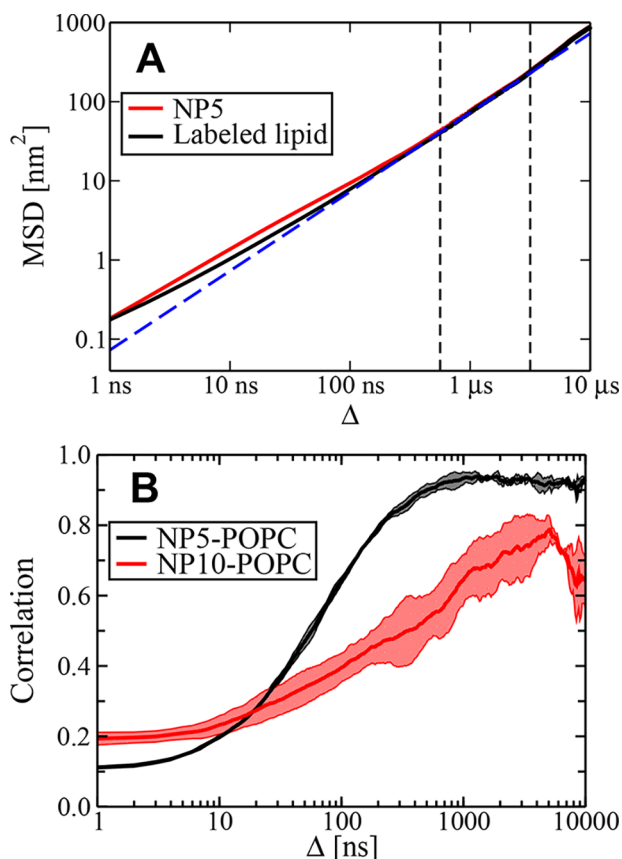


Figure 5. (A) MSDs of the labeled lipid (black line) and the 5 nm NP (red line) as a function of lag time Δ (log–log plot). The dashed blue line demonstrates the expected long-time behavior of normal diffusion, where $\text{MSD} \propto \Delta^1$; the MSDs were averaged over three independent simulations (50 μs each). (B) Correlation between the displacements of the probe lipid and the NP as a function of lag time Δ (semilog plot). Shown are the results for the NP5–POPC (black line) and NP10–POPC (red line) systems.

effect is somewhat surprising because it is not related to the nanoparticle at all. Our results demonstrate that the sAv linker slows down the diffusion of the biotinylated lipid probe even if this linker is not bound to a AuNP. This effect arises from the affinity of lipids for sAv, which binds to about a dozen lipids that are right under the sAv tetramer. The biotinylated probe lipid bound to sAv then moves together with a dozen neighboring lipids surrounding the lipid–sAv complex, and this slows down the diffusion of the probe lipid to a significant degree. The observed effect is likely not sAv-specific and can be expected when the linker agent of an optical label interacts favorably with the lipid membrane. To make the situation more complex, the nanoparticle also slows down the diffusion. This effect arises from frictional drag of a nanoparticle moving in a viscous medium (water) and is dependent on the size of the AuNP: the larger the hydrodynamic radius of the nanoparticle, the more it slows down the lateral motion. However, this effect is likely exaggerated in our simulations due to the limitations of the used coarse-grained model. Furthermore, for larger nanoparticles that accommodate several sAv tetramers, one has additional interactions of nonlinker sAvs with the membrane surface, which potentially could lead to multivalent labeling of the probe lipid. While these artifacts related to sAv tetramers on the AuNP surface cannot be avoided, their effect can be minimized by reducing the NP size down to about 5 nm; nanoparticles in this size range can host no more than one sAv tetramer to interact with the membrane. The use of small nanoparticles (in the ballpark of about 5 nm) is also supported by our studies that unraveled the correlation between the motions of the AuNP and the probe lipid. We found that the trajectory of the AuNP matches the trajectory of the probe lipid only if images of the AuNP position are taken sufficiently rarely. The most accurate temporal resolution is achieved with the smallest nanoparticles and is about one image per microsecond. If the NP size is increased, the temporal resolution decreases.

Concluding, the results presented in this work show that the artifacts in SPT experiments based on the use of biotin- and sAv-linked AuNPs can be minimized by AuNPs in the size range of about 5 nm. Nanoparticles of this size also provide the best temporal resolution.

■ ASSOCIATED CONTENT

■ Supporting Information

The Supporting Information is available free of charge on the ACS Publications website at DOI: 10.1021/acs.jpcl.9b00065.

Model and simulation details and additional analysis and results (PDF)

■ AUTHOR INFORMATION

Corresponding Author

*E-mail: a.gurtovenko@biosimu.org. Web: biosimu.org. Phone: +7-812-3285601. Fax: +7-812-3286869.

ORCID

Andrey A. Gurtovenko: 0000-0002-9834-1617

Matti Javanainen: 0000-0003-4858-364X

Fabio Lolicato: 0000-0001-7537-0549

Ilpo Vattulainen: 0000-0001-7408-3214

Notes

The authors declare no competing financial interest.

■ ACKNOWLEDGMENTS

This work was supported by the Academy of Finland (A.A.G), its Centre of Excellence program (M.J., F.L., I.V.), the European Research Council (I.V.), the Magnus Ehrnrooth Foundation (F.L), and the Emil Aaltonen Foundation (M.J.). For computational resources, we wish to thank the CSC — IT Center for Science (Espoo, Finland).

■ REFERENCES

- (1) Lodish, H.; Berk, A.; Zipursky, S. L.; Matsudaira, P.; Baltimore, D.; Darnell, J. E. *Molecular Cell Biology*; W. H. Freeman and Company: New York, 2000.
- (2) Laganowsky, A.; Reading, E.; Allison, T. M.; Ulmschneider, M. B.; Degiacomi, M. T.; Baldwin, A. J.; Robinson, C. V. Membrane proteins bind lipids selectively to modulate their structure and function. *Nature* **2014**, *510*, 172–175.
- (3) Whitelegge, J. Up close with membrane lipid-protein complexes. *Science* **2011**, *334*, 320–321.
- (4) Almeida, P. F. F.; Vaz, W. L. C. In *Handbook of Biological Physics*; Lipowski, R., Sackmann, E., Eds.; Elsevier: Amsterdam, The Netherlands, 1995; Chapter 6, pp 305–357.
- (5) Phillips, R.; Ursell, T.; Wiggins, P.; Sens, P. Emerging roles for lipids in shaping membrane-protein function. *Nature* **2009**, *459*, 379–385.
- (6) Saxton, M. J. Single-particle tracking: connecting the dots. *Nat. Methods* **2008**, *5*, 671–672.
- (7) Kusumi, A.; Tsunoyama, T. A.; Hirose, K. M.; Kasai, R. S.; Fujiwara, T. K. Tracking single molecules at work in living cells. *Nat. Chem. Biol.* **2014**, *10*, 524–532.
- (8) Manzo, C.; Garcia-Parajo, M. F. A review of progress in single particle tracking: from methods to biophysical insights. *Rep. Prog. Phys.* **2015**, *78*, 124601.
- (9) Shen, H.; Tauzin, L. J.; Baiyasi, R.; Wang, W.; Moringo, N.; Shuang, B.; Landes, C. F. Single particle tracking: From theory to biophysical applications. *Chem. Rev.* **2017**, *117*, 7331–7376.
- (10) Clausen, M. P.; Lagerholm, B. C. The probe rules in single particle tracking. *Curr. Protein Pept. Sci.* **2011**, *12*, 699–713.
- (11) Spillane, K. M.; Ortega-Arroyo, J.; de Wit, G.; Eggeling, C.; Ewers, H.; Wallace, M. I.; Kukura, P. High-speed single-particle tracking of GM1 in model membranes reveals anomalous diffusion due to interleaflet coupling and molecular pinning. *Nano Lett.* **2014**, *14*, 5390–5397.
- (12) Hsieh, C. L.; Spindler, S.; Ehrig, J.; Sandoghdar, V. Tracking single particles on supported lipid membranes: Multimobility diffusion and nanoscopic confinement. *J. Phys. Chem. B* **2014**, *118*, 1545–1554.
- (13) Spindler, S.; Ehrig, J.; Konig, K.; Nowak, T.; Piliarik, M.; Stein, H. E.; Taylor, R. W.; Garanger, E.; Lecommandoux, S.; Alves, I. D.; et al. Visualization of lipids and proteins at high spatial and temporal resolution via interferometric scattering (iSCAT) microscopy. *J. Phys. D: Appl. Phys.* **2016**, *49*, 274002.
- (14) Wu, H. M.; Lin, Y. H.; Yen, T.-C.; Hsieh, T. C. Y. Nanoscopic substructures of raft-mimetic liquid-ordered membrane domains revealed by high-speed single-particle tracking. *Sci. Rep.* **2016**, *6*, 20542.
- (15) Lin, Y. H.; Chang, W. L.; Hsieh, C. L. Shot-noise limited localization of single 20 nm gold particles with nanometer spatial precision within microseconds. *Opt. Express* **2014**, *22*, 9159–9170.
- (16) Marrink, S. J.; Risselada, H. J.; Yefimov, S.; Tieleman, D. P.; de Vries, A. H. The MARTINI force field: Coarse grained model for biomolecular simulations. *J. Phys. Chem. B* **2007**, *111*, 7812–7824.
- (17) Monticelli, L.; Kandasamy, S. K.; Periole, X.; Larson, R. G.; Tieleman, D. P.; Marrink, S. J. The MARTINI Coarse-grained force field: Extension to proteins. *J. Chem. Theory Comput.* **2008**, *4*, 819–834.
- (18) de Jong, D. H.; Singh, G.; Bennett, W. F. D.; Arnarez, C.; Wassenaar, T. A.; Schafer, L. V.; Periole, X.; Tieleman, D. P.; Marrink,

S. J. Improved parameters for the Martini coarse-grained protein force field. *J. Chem. Theory Comput.* **2013**, *9*, 687–697.

(19) Abraham, M. J.; Murtola, T.; Schulz, R.; Pall, S.; Smith, J.; Hess, B.; Lindahl, E. Gromacs: high performance molecular simulations through multi-level parallelism from laptops to supercomputers. *SoftwareX* **2015**, *1–2*, 19–25.

(20) de Jong, D. H.; Baoukina, S.; Ingolfsson, H. I.; Marrink, S. J. Martini straight: Boosting performance using a shorter cutoff and GPUs. *Comput. Phys. Commun.* **2016**, *199*, 1–7.

(21) Javanainen, M.; Martinez-Seara, H.; Metzler, R.; Vattulainen, I. Diffusion of integral membrane proteins in protein-rich membranes. *J. Phys. Chem. Lett.* **2017**, *8*, 4308–4313.

(22) Jeon, J. H.; Javanainen, M.; Martinez-Seara, H.; Metzler, R.; Vattulainen, I. Protein crowding in lipid bilayers gives rise to non-Gaussian anomalous lateral diffusion of phospholipids and proteins. *Phys. Rev. X* **2016**, *6*, 021006.

(23) Niemela, P. S.; Miettinen, M. S.; Monticelli, L.; Hammaren, H.; Bjelkmar, P.; Murtola, T.; Lindahl, E.; Vattulainen, I. Membrane proteins diffuse as dynamic complexes with lipids. *J. Am. Chem. Soc.* **2010**, *132*, 7574–7575.

(24) Saffman, P.; Delbruck, M. Brownian motion in biological membranes. *Proc. Natl. Acad. Sci. U. S. A.* **1975**, *72*, 3111–3113.

(25) Camley, B. A.; Lerner, M. G.; Pastor, R. W.; Brown, F. L. H. Strong influence of periodic boundary conditions on lateral diffusion in lipid bilayer membranes. *J. Chem. Phys.* **2015**, *143*, 243113.

(26) Venable, R. M.; Ingolfsson, H. I.; Lerner, M. G.; Perrin, B. S., Jr.; Camley, B. A.; Marrink, S. J.; Brown, F. L. H.; Pastor, R. W. Lipid and peptide diffusion in bilayers: The Saffman-Delbruck model and periodic boundary conditions. *J. Phys. Chem. B* **2017**, *121*, 3443–3457.

(27) Vögele, M.; Köfinger, J.; Hummer, G. Hydrodynamics of diffusion in lipid membrane simulations. *Phys. Rev. Lett.* **2018**, *120*, 268104.

(28) Vögele, M.; Hummer, G. Divergent diffusion coefficients in simulations of fluids and lipid membranes. *J. Phys. Chem. B* **2016**, *120*, 8722–8732.

(29) Fujiwara, T.; Ritchie, K.; Murakoshi, H.; Jacobson, K.; Kusumi, A. Phospholipids undergo hop diffusion in compartmentalized cell membrane. *J. Cell Biol.* **2002**, *157*, 1071–1081.

(30) Reina, F.; Galiani, S.; Shrestha, D.; Sezgin, E.; de Wit, G.; Cole, D.; Lagerholm, B. C.; Kukura, P.; Eggeling, C. Complementary studies of lipid membrane dynamics using iSCAT and super-resolved fluorescence correlation spectroscopy. *J. Phys. D: Appl. Phys.* **2018**, *51*, 235401.

(31) Kusumi, A.; Nakada, C.; Ritchie, K.; Murase, K.; Suzuki, K.; Murakoshi, H.; Kasai, R. S.; Kondo, J.; Fujiwara, T. Paradigm shift of the plasma membrane concept from the two-dimensional continuum fluid to the partitioned fluid: High-speed single-molecule tracking of membrane molecules. *Annu. Rev. Biophys. Biomol. Struct.* **2005**, *34*, 351–378.

(32) Weigel, A. V.; Simon, B.; Tamkun, M. M.; Krapf, D. Ergodic and nonergodic processes coexist in the plasma membrane as observed by single-molecule tracking. *Proc. Natl. Acad. Sci. U. S. A.* **2011**, *108*, 6438–6443.